Model Discrepancy Learning for Heat Exchanger Networks

Akan, M. Tolga; Portilla, Christian; Özkan, Leyla

DOI
10.1016/j.ifacol.2024.08.348

Publication date
2024

Document Version
Final published version

Published in
IFAC-PapersOnLine

Available online at www.sciencedirect.com

ScienceDirect

IFAC PapersOnline CONFERENCE PAPER ARCHIVE

IFAC PapersOnLine 58-14 (2024) 271–276

Model Discrepancy Learning for Heat Exchanger Networks ⋆

M. Tolga Akan[1] **Christian Portilla**[1] **Leyla Özkan**[1,2]

[1] *Eindhoven University of Technology, Eindhoven, The Netherlands*
[2] *Delft University of Technology, Delft, The Netherlands*
(e-mail: {m.t.akan, c.r.portilla, l.ozkan}@tue.nl, lozkan@tudelft.nl).

Abstract: In the heat treatment processes, offline utilization of first-principles models is well-established. These models tend to be complex, computationally demanding, and rely heavily on empirical relations. The fidelity of these models degrades over time due to changes in the process resulting in plant-model mismatch, which is typically attributed to an incorrect constitutive relation of a physical mechanism in the model (i.e. fouling in the heat exchangers). In this paper, we propose two hybrid modeling approaches, namely Sparse Identification of Nonlinear Dynamics with Control and least square estimation, to learn the dynamics of the discrepancy between the measurement data and the simulation model. The hybrid modeling approach is implemented on a heat exchanger network (HEN) example and it is shown that the accuracy of the first principles dynamic model is improved.

Keywords: hybrid modeling, sparse identification, model discovery, heat exchanger fouling

1. INTRODUCTION

Process systems inevitably degrade over time, leading to reduced production performance and quality. Regular checks of component health and performance indicators are required. However, in cases where the degradation process is complex due to limited prior knowledge about its mechanism, deriving a robust fouling model based on first principles becomes challenging. Furthermore, the worldwide total cost of fouling in industrial operations is estimated to be in the order of $0.1 - 0.3\%$ of the Gross National Product (Boxler (2014)), and Bansal and Chen (2006) indicate that in the dairy industry, the total cost of the fouling and fouling-related cleaning processes is about 80% of the total production cost.

Traditionally, degradation assessment in process industry involves observing relevant states linked to the degradation mechanism. Methods like the Extended Kalman Filter (EKF) can monitor the evolution of parameters related to fouling (Jonsson et al. (2007)). However, solely observing process states isn't sufficient for accurate future predictions; it is crucial to comprehensively model the entire process by uncovering unknown degradation mechanisms.

Given the complexity of degradation mechanisms, a data-driven (DD) model is often preferred for discovering degradation dynamics. However, it still necessitates prior knowledge of the degradation physics. Hybrid modeling (HM), which combines DD and first principles (FPs) approaches, addresses this challenge (Rajulapati et al. (2022)). In cases where FPs are only partially known, approaches like residual modeling and FP-constrained modeling are commonly employed. For instance, a recent study by Kaheman et al. (2019) proposes an HM approach using DD methods to discover the discrepancy model between known FPs and measurement data. Techniques such as sparse identification of nonlinear dynamics (SINDYc) (Brunton et al. (2016)) and deep learning for model discovery (DeepMoD) Both et al. (2021) are examples of this approach, as they utilize sparse estimation over a broad range of candidate basis functions for model discovery.

In this work, we assume that the consecutive equations related to the thermal interactions in the heat exchanger are well-known. In contrast, the equation(s) related to the heat exchanger fouling dynamics are unknown. Hence, a discrepancy between the prediction based on the available model and the plant measurements occurs.

To this end, we employ the residual modeling approach to minimize the discrepancy between the measured data and the available model. As it is elucidated in Ebers et al. (2022), various modeling frameworks would be used to disambiguate the (un-) deterministic effects of the discrepancy via SINDY, Dynamic Mode Decomposition (DMD) of Tu (2013), Gaussian Process Regression (GPR) of Rasmussen (2003), and Neural Networks (NN). Out of these methods, it is reported that SINDY has the lowest computational cost, whereas NN has the highest. On the other hand, DMD - a linear model discovery method - struggles to create an accurate discrepancy model resulting in lower forecasting performance as the nonlinear parameters increase.

Considering these, we use SINDYc-based hybrid modeling Kaheman et al. (2019) with the Complementary Pairs Stability Selection (CPSS) method Shah and Samworth

⋆ This publication is part of an Institute for Sustainable Process Technology (ISPT) project: The Heat is On (THIO), and is executed with subsidy of Topsector Energy of the Dutch Ministry of Economic Affairs and Climate Policy, executed by the Netherlands Enterprise Agency (RVO). The specific subsidy for this project is MOOI-subsidy 2020.

10.1016/j.ifacol.2024.08.348

(2012) for developing a residual model. Furthermore, we propose another hybrid model based on the least square estimation method. With these hybrid modeling approaches a model with improved forecasting performance is obtained.

In this paper, Section 2, presents the background information on the hybrid modeling approach. Section 3, discusses the problem by introducing the enthalpy-based modeling of a fouled counter-flow heat exchanger network and the fouling model discovery methodology based on the residual modeling strategy. The results of the simulations are presented in Section 4. Finally, the conclusion and perspectives are derived in Section 5.

2. BACKGROUND INFORMATION

2.1 Sparse Identification of Nonlinear Dynamics for Control

We consider the nonlinear dynamical system

$$\dot{\boldsymbol{x}}(t) = \boldsymbol{f}(\boldsymbol{x}(t), \boldsymbol{u}(t); \boldsymbol{\mu}), \tag{1}$$

with state $\boldsymbol{x}(t) = [x_1(t) \dots x_n(t)] \in \mathbb{R}^n$, control input $\boldsymbol{u}(t) = [u_1(t) \dots u_q(t)] \in \mathbb{R}^q$, parameters set $\boldsymbol{\mu}$, and smooth dynamics $\boldsymbol{f}(\boldsymbol{x}(t), \boldsymbol{u}(t); \boldsymbol{\mu}) : \mathbb{R}^n \times \mathbb{R}^q \to \mathbb{R}^n$. Let $\mathbf{X} \in \mathbb{R}^{m \times n}$ and $\mathbf{U} \in \mathbb{R}^{m \times q}$ are the states and inputs dataset made of m measured time steps of the state $\boldsymbol{x}(t)$ and input signal $\boldsymbol{u}(t)$. The time derivatives $\dot{\mathbf{X}} \in \mathbb{R}^{m \times n}$, if not measured directly, are computed by numerical differentiation.

The system in Eq. (1) can thus be approximated as:

$$\dot{\mathbf{X}} \approx \Theta(\mathbf{X}, \mathbf{U})\boldsymbol{\xi}, \tag{2}$$

where a large basis functions library $\Theta(\mathbf{X}, \mathbf{U})$ and sparse coefficients vector $\boldsymbol{\xi}$ represent the parameters that make the linear combinations of basis functions the true system.

However, for most of the dynamical systems, the complete system dynamics - ODE structure - is unknown. Based on this representation, an unknown ODE structure corresponds to having an unknown sparse vector $\boldsymbol{\xi}$ for a specific library $\Theta(\mathbf{X}, \mathbf{U})$. This unknown sparse vector can be estimated using sparsity estimators. For example, Lasso ($\ell_1 - norm$ regularized least-square minimization) can be employed for this purpose:

$$\boldsymbol{\xi} = \underset{\boldsymbol{\xi}}{\operatorname{argmin}} \Big(\left\| \dot{\mathbf{X}} - \Theta(\mathbf{X}, \mathbf{U})\boldsymbol{\xi} \right\|_2 + \lambda \left\| \boldsymbol{\xi} \right\|_1 \Big). \tag{3}$$

Using this method, a sparse $\boldsymbol{\xi}$ corresponding to the optimal linear combinations of the basis functions in library $\Theta(\mathbf{X}, \mathbf{U})$ that gives good model performance can be identified by tuning the penalization parameter - λ - using k-fold cross-validation.

However, even optimal tuning of λ cannot distinguish between signal variables and noise variables in most of the cases. To address this problem Meinshausen and Buhlmann (2010) introduced a promising variable selection method called Stability Selection (SS). The SS algorithm computes a stability measure for each variable based on its frequency of selection in bootstrapped estimations. Variables with stability measures below a predefined threshold are filtered out, leading to an improved variable selection performance of the base estimator. Moreover, this method exhibits low sensitivity to the choice of the regularization parameter. In our research, we use an enhanced extension of SS, named Complementary Pairs Stability Selection (CPSS) algorithm (Shah and Samworth, 2012) instead of Lasso in Eq. 3.

2.2 Hybrid Modeling via Residual Modeling

Consider a dynamical system, $\boldsymbol{f}_o$

$$\dot{\boldsymbol{x}}^{\mathbf{0}}(t) = \boldsymbol{f}_o\left(\boldsymbol{x}^0(t), \boldsymbol{u}(t); \boldsymbol{\mu}_o\right). \tag{4}$$

The mechanistic model output for this system is given as

$$\dot{\boldsymbol{x}}^M(t) = \boldsymbol{f}_m\left(\boldsymbol{x}(t), \boldsymbol{u}(t); \boldsymbol{\mu}_m\right), \tag{5}$$

where the noisy measurement is $\boldsymbol{x}(t) = \boldsymbol{x}^0(t) + \epsilon$.

Parameter error, $\boldsymbol{\mu}_o \neq \boldsymbol{\mu}_m$, model inadequacy, $\boldsymbol{f}_o \neq \boldsymbol{f}_m$, and measurement noise contribute to the plant-model mismatch, expressed as:

$$\begin{aligned} \delta\dot{\boldsymbol{x}}(t) =& \dot{\boldsymbol{x}}(t) - \dot{\boldsymbol{x}}^M(t) \\ =& \boldsymbol{f}_o(\boldsymbol{x}(t), \boldsymbol{u}(t); \boldsymbol{\mu}_o) - \boldsymbol{f}_m\left(\boldsymbol{x}(t), \boldsymbol{u}(t); \boldsymbol{\mu}_m\right) \end{aligned} \tag{6}$$

We collect the error data from a model and represent it as a matrix, denoted as $\delta\dot{\mathbf{X}} = [\delta\dot{\boldsymbol{x}}(t_1) \dots \delta\dot{\boldsymbol{x}}(t_m)]^\top \in \mathbb{R}^{m \times n}$.

Next, we construct a library of candidate functions $\Theta(\mathbf{X}, \mathbf{U})$. Our choice of functions in this library is typically based on our prior knowledge about the (sub)model of the discrepancy.

The problem of finding a sparse representation is then formulated as follows:

$$\delta\dot{\mathbf{X}} \approx \boldsymbol{\Theta}(\boldsymbol{X}, \boldsymbol{U})\boldsymbol{\xi}.$$

To sparsely represent the discrepancy model using the given data $\delta\dot{\mathbf{X}}$, $\boldsymbol{X}$ and $\boldsymbol{U}$ by discovering $\boldsymbol{\xi}$, the SINDYc approach or its extension with CPSS can be employed.

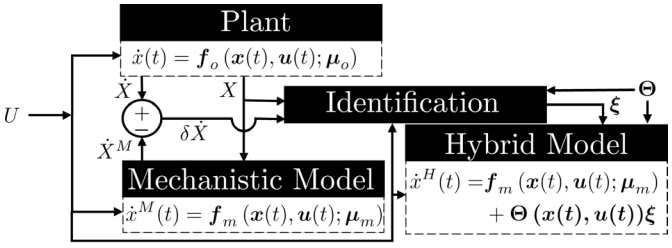

Fig. 1. Compensating the model discrepancy via learning

The graphical representation of the residual modeling approach is presented in Fig. 1. The identification box represents the identification method that takes the system states, inputs, and the difference between the mechanistic model's estimated state derivatives and the true system state derivatives to learn the discrepancy dynamics between the true system and the mechanistic model. Later, the discovered discrepancy dynamics are used to compensate for the mechanistic model to create a hybrid model.

3. PROBLEM FORMULATION

Initially, we present the true model of the system based on an enthalpy-based counter-flow heat exchanger network modeling with milk fouling effects incorporated. Subsequently, we describe the discrepancies in the mechanistic model resulting from the inadequate incorporation of the fouling effect into the process. Later we employ two data-driven methods to characterize the discrepancy dynamics.

3.1 Enthalpy Based Heat Exchanger Modeling

We consider a counter-flow heat exchanger (CFHEX) model based on the enthalpy dynamics modeling approach of Zitte et al. (2018) and assume that the tube and shell components have constant volumes (V and $\bar{V}$ $[m^3]$), densities (ρ and $\bar{\rho}$ $[kg/m^3]$) and pressures (P and $\bar{P}$ $[kg/m^3]$).

As a result of these assumptions PV remains constant which results in no delay in inlet/outlet flow rates and the total energy of the compartments is equal to the enthalpy of the compartments. Considering that the total amount of enthalpy in the $(i,j)^{th}$ compartments are given by:

$$\begin{aligned} H_{i,j} &= \rho V h(T_{i,j}), \quad h(T_{i,j}) = c_p(T_{i,j} - T_{ref}) + h_{ref}, \\ \bar{H}_{i,j} &= \bar{\rho}\bar{V} h(\bar{T}_{i,j}), \quad h(\bar{T}_{i,j}) = \bar{c}_p(T_{i,j} - T_{ref}) + h_{ref}, \end{aligned} \tag{7}$$

where h (J/kg) is the specific enthalpy and $T_{i,j}$ and $\bar{T}_{i,j}$ (K) are the temperatures of the $(i,j)^{th}$ compartments of the cold and hot ports.

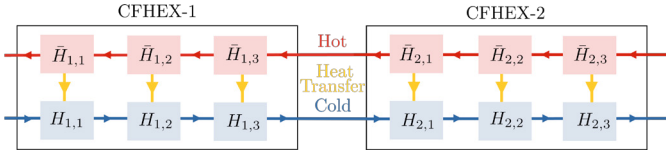

Fig. 2. Graph representation of CFHEXs in series where the number of sections (ns) and CFHEXs (nh) are 3 and 2, respectively. Red, blue, and orange ports represent the hot water in the shell, the cold milk in the tube, and the heat transfer, respectively.

$\bar{H}_{i,j}$ and $H_{i,j}$ are the enthalpy in the section j of HEX i for hot and cold fluids. A nonlinear dynamic model for a heat exchanger is given by the enthalpy balance:

$$\begin{aligned} \frac{d}{dt}\bar{H}_{i,j}(t) = &-\lambda_{i,j}(t)\left[\left(\frac{\bar{H}_{i,j}(t)}{\bar{\rho}\bar{V}\bar{c}_p} - \frac{h_{ref}}{\bar{c}_p}\right) - \left(\frac{H_{i,j}(t)}{\rho V c_p} - \frac{h_{ref}}{c_p}\right)\right] \\ &+ \bar{Q}(t)\left(\bar{h}^{in}_{i,j}(t) - \frac{\bar{H}_{i,j}(t)}{\bar{\rho}\bar{V}}\right), \\ \frac{d}{dt}H_{i,j}(t) = &\ \lambda_{i,j}(t)\left[\left(\frac{\bar{H}_{i,j}(t)}{\bar{\rho}\bar{V}\bar{c}_p} - \frac{h_{ref}}{\bar{c}_p}\right) - \left(\frac{H_{i,j}(t)}{\rho V c_p} - \frac{h_{ref}}{c_p}\right)\right] \\ &+ Q(t)\left(h^{in}_{i,j}(t) - \frac{H_{i,j}(t)}{\rho V}\right), \end{aligned} \tag{8}$$

where $1 \le j \le ns$ and $1 \le i \le nh$, $h^{in}_{i,j}(t) = \frac{H_{i,j-1}(t)}{\rho V}$ for $2 \le j \le ns$ and $\bar{h}^{in}_{i,j}(t) = \frac{\bar{H}_{i,j+1}(t)}{\bar{\rho}\bar{V}}$ for $1 \le j \le ns-1$, $\lambda_{i,j}(t)$ (W/K) is the overall heat exchange coefficient, Q (kg/s) is the mass flow rate, the subscript in refers to the inlet, and the bar, $\bar{\cdot}$, refers to the variables on the shell side of the heat exchanger while no bar indicates the tube side.

In 8, we also have:

$$\lambda_{i,j}(t) = \frac{1}{\frac{1}{\lambda_0} + R^f_{i,j}(t)}, \tag{9}$$

where λ_0 is the heat transfer coefficient of both fluids and $R_{i,j}(t)$ is the thermal resistance of the fouling for j^{th} section of HEX i. Note that if there is no fouling, $R_{i,j}(t) = 0$, and $\lambda_{i,j} = \lambda_0$.

We consider a fouling model for milk at Ultra-High-Temperature (UHT) pasteurization proposed by Fryer (1988) that simply represents a nucleation-and-growth process and correlates as a function of surface temperature $(T^s_{i,j}(t))$ and the Reynolds number $(Re_{i,j}(t))$:

$$\frac{d}{dt}Bi_{i,j}(t) = \frac{k_d}{Re_{i,j}(t)} e^{\frac{-E}{RT^s_{i,j}(t)}} - k_r Bi_{i,j}(t), \tag{10}$$

where $Bi_{i,j}(t) = \lambda_0 R^f_{i,j}(t)$ is the Biot number, k_d and k_r are deposition and removal rate constants, the reaction activation energy (J/mol), R is the universal gas constant (J/(mol K)). The surface temperature is calculated as:

$$T^s_{i,j}(t) = 0.5\left(T_{i,j}(t) + \bar{T}_{i,j}(t)\right).$$

One can also represent the fouling model in Eq. 10 as:

$$\frac{d}{dt}R^f_{i,j}(t) = \frac{k_d}{\lambda_0 Re_{i,j}(t)} e^{-\frac{E}{RT^s_{i,j}}} - k_r R^f_{i,j}(t) \tag{11}$$

It is assumed that the fouling only occurs in the cold fluid (i.e. the inner pipe). Hence, the Reynolds number for the cold fluid is calculated as:

$$Re_{i,j}(t) = \frac{4Q_{i,j}(t)}{\pi D \nu} \tag{12}$$

where D is the diameter of the pipe (m), ν is the kinematic viscosity (Pas).

3.2 Discrepancy in HEN Model

We address the process uncertainty arising from the inadequate modeling of the dynamic system in the mechanistic model. The reason for such uncertainty is the complex dynamics of the varying λ parameters which are functions of the fouling. We propose to enhance the available mechanistic model by learning the model of the discrepancy - $\delta\dot{x}_{i,j}(t)$ - between the available mechanistic (with superscript M) model $\dot{x}^M_{i,j}(t)$ and the observed value $\dot{x}_{i,j}(t)$.

Consider the true dynamical system -f_0- given as:

$$\dot{x}^0_{i,j} = f_o(x^0_{i,j}(t), u_{i,j}(t); \mu_o) \tag{13}$$

where the state of the section j of HEX i at time t is given by $x^0_{i,j}(t) = \left[\bar{H}^0_{i,j}(t), H^0_{i,j}(t)\right]^T$ and $u_{i,j}(t) = \left[\bar{Q}(t)\bar{h}^{in}_{i,j}, Q(t)h^{in}_{i,j}\right]^T$. For Eq. 8 the true model can be represented as:

$$\begin{aligned} \dot{x}^0_{i,j}(t) = &\left(\lambda_{i,j}(t)\begin{bmatrix} \frac{-1}{\bar{\rho}\bar{V}\bar{c}_p} & \frac{1}{\rho V c_p} \\ \frac{1}{\bar{\rho}\bar{V}\bar{c}_p} & \frac{-1}{\rho V c_p} \end{bmatrix} + \begin{bmatrix} \frac{-\bar{Q}(t)}{\bar{\rho}\bar{V}\bar{c}_p} & 0 \\ 0 & \frac{-Q(t)}{\rho V c_p} \end{bmatrix}\right) x^0_{i,j}(t) \\ &+ \lambda_{i,j}(t) h_{ref}\left(\frac{1}{c_p} - \frac{1}{\bar{c}_p}\right)\begin{bmatrix} -1 \\ 1 \end{bmatrix} + u_{i,j}(t) \end{aligned} \tag{14}$$

The states of the system and their derivatives sampled at times $t_1, ..., t_m$ are given by: $X_{i,j} = [x_{i,j}(t_1) \ \dots \ x_{i,j}(t_m)]^T$ and $\dot{X}_{i,j} = [\dot{x}_{i,j}(t_1) \ \dots \ \dot{x}_{i,j}(t_m)]^T$ where $x_{i,j}(t)$ is the noisy measurement as $x_{i,j}(t) = x^0_{i,j}(t) + \epsilon$.

Assume that the given structure of the Ordinary Differential Equation (ODE) that describes the process in HEX and the geometric information of the HEX are known whereas no information about the true fouling model is available. The mechanistic model is represented with no fouling $(R_{i,j}(t) = 0)$. Hence, we can represent the mechanistic model output for this system as:

$$\dot{x}^{\mathrm{M}}_{i,j}(t) = f_m(x_{i,j}(t), u_{i,j}(t); \mu_m). \tag{15}$$

Similarly, the mechanistic model takes the form of Eq. 14 with $\lambda_{i,t}(t) = \lambda_0$.

The states of the system and their derivatives sampled at times $t_1, ..., t_m$ that are estimated by the mechanistic model are given by: $\dot{X}^{\mathrm{M}}_{i,j} = [\dot{x}^{\mathrm{M}}_{i,j}(t_1) \ \dots \ \dot{x}^{\mathrm{M}}_{i,j}(t_m)]^\top$.

The model discrepancy, $\delta x(t)$, can be expressed by subtracting Eq. 15 from Eq. 8 and taking $h_{ref} = 0$.

This is given as:

$$\begin{aligned}\delta\dot{x}_{i,j}(t) =& \dot{x}_{i,j}(t) - \dot{x}^{M}_{i,j}(t) \\ =& \delta\lambda_{i,j}(t) \begin{bmatrix} \frac{-1}{\bar{\rho}\bar{V}\bar{c}_p} & \frac{1}{\rho V c_p} \\ \frac{1}{\bar{\rho}\bar{V}\bar{c}_p} & \frac{-1}{\rho V c_p} \end{bmatrix} x_{i,j}(t),\end{aligned} \tag{16}$$

where

$$\delta\lambda_{i,j}(t) = \lambda_{i,j}(t) - \lambda_o = \frac{\lambda_o}{1 + \lambda_o R^f_{i,j}(t)} - \lambda_o$$

in which $R^f_{i,j}(t)$ is the fouling resistance and it is function of $Re_{i,j}(t)$ and $T^s_{i,j}(t)$.

Using the relations in Eq. 7, Eq. 16 can be rewritten and it can be simply represented as a function of the temperature difference between compartments:

$$\begin{aligned}\delta\dot{x}_{i,j}(t) =& \delta\lambda_{i,j}(t) \begin{bmatrix} -\bar{T}_{i,j}(t) + T_{i,j}(t) \\ \bar{T}_{i,j}(t) - T_{i,j}(t) \end{bmatrix} \\ =& \delta\lambda_{i,j}(t)\Delta T_{i,j}(t) \begin{bmatrix} -1 \\ +1 \end{bmatrix}.\end{aligned} \tag{17}$$

By simply subtracting the mechanistic model output from the measured output, we can have the model error data as:

$$\delta\dot{X}_{i,j} = [\delta\dot{x}_{i,j}\,(t_1) \quad \dots \quad \delta\dot{x}_{i,j}\,(t_m)]^T = \dot{X}_{i,j} - \dot{X}^{\mathrm{M}}_{i,j}.$$

The only prior information considered is that the dynamics of $\delta\lambda_{i,j}(t)$ depend on the values of $T^s_{i,j}(t)$ and $Re_{i,j}(t)$. The surface temperatures are not measured values, but they can be calculated for each pair of compartments using Eq. 7. Similarly, the Reynolds numbers for the cold pipe can be calculated using the Eq. 12.

Keep in mind, that the temperature difference vector ($\mathbf{\Delta T}_{i,j}$), the surface temperatures vector ($\mathbf{T^s}_{i,j}$), the Reynolds numbers vector ($\mathbf{Re}_{i,j}$), the flowrate vector of the cold fluid ($\mathbf{Q}_{i,j}$), and the time vector $\mathbf{t}$ are all sampled at times, $t_1, ..., t_m$.

3.3 Hybrid Model I (HM I): Discrepancy Identification via SINDYc with CPSS

By processing the measured data, we can have $\delta\dot{X}_{i,j}$, $\mathbf{\Delta T}_{i,j}$ $\mathbf{T^s}_{i,j}$, and $\mathbf{Re}_{i,j}$ with these we can approximate $\delta\dot{X}_{i,j}$ using a candidate function library $\Theta(\mathbf{\Delta T}_{i,j}, \mathbf{T^s}_{i,j}, \mathbf{Re}_{i,j})$ and the sparse parameter vector of the corresponding features $\boldsymbol{\xi}$.

If the data matrix is populated with relevant enough candidate functions, the model discrepancy measurement can be approximated as multiplication of the data matrix via a sparse matrix as:

$$\delta\dot{X}_{i,j} \approx \Theta(\mathbf{\Delta T}_{i,j}, \mathbf{T^s}_{i,j}, \mathbf{Re}_{i,j})\boldsymbol{\xi}. \tag{18}$$

Accuracy of the approximation of $\delta\dot{X}_{i,j}$ via Eq. 18 depends on design of the data matrix, $\Theta(\mathbf{\Delta T}_{i,j}, \mathbf{T^s}_{i,j}, \mathbf{Re}_{i,j})$.

Therefore, we propose to approximate the model discrepancy - L.H.S. of Eq. 16 - with the basis functions inspired by the function on the R.H.S. of the same equation. This is achieved by choosing the columns of the data matrix using Eq. 16 with different base functions $\delta\lambda_{i,j,k}(t)$ as:

$$\Theta(\mathbf{\Delta T}_{i,j}, \mathbf{T^s}_{i,j}, \mathbf{Re}_{i,j}) = [\theta_1 \cdots \theta_k \cdots \theta_p], \tag{19}$$

$$\begin{aligned}\text{where } \theta_k =& [\theta_k(t_1), \cdots, \theta_k(t_m)]^T, \\ \text{with } \theta_k(t) =& \delta\lambda_{i,j,k}(t)\Delta T_{i,j}(t) \begin{bmatrix} -1 \\ +1 \end{bmatrix},\end{aligned}$$

where the candidate functions for the overall heat transfer coefficient discrepancy - $\delta\lambda_{i,j,k}(t)$ - are chosen from the set $\boldsymbol{\delta\lambda}^{set}_{i,j}(t) = \{\delta\lambda_{i,j,1}(t), \cdots, \delta\lambda_{i,j,k}(t), \cdots, \delta\lambda_{i,j,p}(t)\}$. We describe $\delta\lambda_{i,j}(t)$ as exponential functions that resemble Arrhenius equations with functions of $\mathbf{T^s}_{i,j}$ and $\mathbf{Re}_{i,j}$:

$$\delta\lambda_{i,j}(t) \approx \sum_{k=0}^{K} a_k e^{b_k T^s_{i,j}(t)} + Re_{i,j}(t) \sum_{l=0}^{L} c_l e^{d_l T^s_{i,j}(t)}. \tag{20}$$

The exponential functions proposed in Eq. 20 can be defined by infinite summation of the power series as:

$$\begin{aligned}\delta\lambda_{i,j}(t) \approx& \sum_{k=0}^{K} a_k \sum_{n=0}^{\infty} \frac{\left(b_k T^s_{i,j}(t)\right)^n}{n!} \\ &+ Re_{i,j}(t) \sum_{l=0}^{L} a_l \sum_{n=0}^{\infty} \frac{\left(b_l T^s_{i,j}(t)\right)^n}{n!} \\ \approx& \sum_{n=0}^{\infty} \alpha_n (T^s_{i,j}(t))^n + Re_{i,j} \sum_{n=0}^{\infty} \beta_n (T^s_{i,j}(t))^n.\end{aligned} \tag{21}$$

We create a finite set $\boldsymbol{\delta\lambda}^{set}_{i,j}(t)$, that includes the candidate $\delta\lambda_{i,j,k}(t)$ terms in Eq. 19, using the the power series of $(T^s_{i,j,k}(t))^n$ and $Re_{i,j,k}(t)(T^s_{i,j,k}(t))^n$ with $0 \le n \le 1$.

From Eq. 21 the candidate functions - $\delta\lambda_{i,j,k}(t)$ - are chosen from the set:

$$\boldsymbol{\delta\lambda}^{set}_{i,j}(t) = \{\, 1,\ \boldsymbol{Re}_{i,j}(t),\ \boldsymbol{T}^s_{i,j}(t),\ \boldsymbol{Re}_{i,j}(t)\boldsymbol{T}^s_{i,j}(t) \,\}.$$

By following the above presented library construction method and Eq. 19, the data matrix $\Theta(\mathbf{\Delta T}_{i,j}, \mathbf{T^s}_{i,j}, \mathbf{Re}_{i,j})$ can be constructed. Next, we approximate $\delta\dot{X}_{i,j}$ using the linear combination of the columns of $\Theta(\mathbf{\Delta T}_{i,j}, \mathbf{T^s}_{i,j}, \mathbf{Re}_{i,j})$ with the vector ξ. In order to get the same discrepancy dynamics structure for ξ in a sparse estimation, $\delta\dot{X}_{i,j}$ and $\Theta(\mathbf{\Delta T}_{i,j}, \mathbf{T^s}_{i,j}, \mathbf{Re}_{i,j})$ matrices of different compartments are concatenated to create $\boldsymbol{\delta\dot{X}}$ and $\boldsymbol{\Theta(\Delta T, T^s, Re)}$. For the plant of Fig. 2, the complete discrepancy model can be approximated as:

$$\underbrace{\begin{bmatrix} \delta\dot{X}_{1,1} \\ \delta\dot{X}_{1,2} \\ \delta\dot{X}_{1,3} \\ \delta\dot{X}_{2,1} \\ \delta\dot{X}_{2,2} \\ \delta\dot{X}_{2,3} \end{bmatrix}}_{\boldsymbol{\delta\dot{X}}} \approx \underbrace{\begin{bmatrix} \Theta(\mathbf{\Delta T}_{1,1}, \mathbf{T^s}_{1,1}, \mathbf{Re}_{1,1}) \\ \Theta(\mathbf{\Delta T}_{1,2}, \mathbf{T^s}_{1,2}, \mathbf{Re}_{1,2}) \\ \Theta(\mathbf{\Delta T}_{1,3}, \mathbf{T^s}_{1,3}, \mathbf{Re}_{1,3}) \\ \Theta(\mathbf{\Delta T}_{2,1}, \mathbf{T^s}_{2,1}, \mathbf{Re}_{2,1}) \\ \Theta(\mathbf{\Delta T}_{2,2}, \mathbf{T^s}_{2,2}, \mathbf{Re}_{2,2}) \\ \Theta(\mathbf{\Delta T}_{2,3}, \mathbf{T^s}_{2,3}, \mathbf{Re}_{2,3}) \end{bmatrix}}_{\boldsymbol{\Theta(\Delta T, T^s, Re)}} \boldsymbol{\xi}. \tag{22}$$

The sparse regression problem presented in Eq. 22 can be solved using the CPSS method.

3.4 Hybrid Model II (HM II): Discrepancy Identification via Least Square Estimation

We can also approximate the model discrepancy - L.H.S. of Eq. 16, without constraining ourselves with the basis functions inspired by the function on the R.H.S. of the same equation. This way, HM II can be seen as a baseline for HM I. We propose to approximate L.H.S. of Eq. 16 with a linear combination of 3 basis functions. The first basis function is the difference between the measured temperature in each section $\Delta T_{i,j}(t)$, similar to Eq. 19. The second basis function is the cold flow rate given by the input $Q_{i,j}(t)$ since we assume that fouling only occurs in cold pipe. The last basis function describes the accumulative effect of the fouling employing the time vector, t. Therefore, the discrepancy is approximated as:

$$\delta\dot{X}_{i,j} \approx \boldsymbol{\Theta}(\boldsymbol{\Delta T}_{i,j}, \mathbf{Q}_{i,j}, \mathbf{t})\boldsymbol{\xi}, \tag{23}$$

where

$$\begin{aligned} \boldsymbol{\Theta}(\boldsymbol{\Delta T}_{i,j}, \mathbf{Q}_{i,j}, \mathbf{t}) &= [\theta_1 \quad \theta_2 \quad \theta_3], \\ \text{where } \theta_k &= [\theta_k(t_1), \cdots, \theta_k(t_m)]^T, \\ \text{with } \theta_k(t) &= \delta F_{i,j,k}(t) \begin{bmatrix} -1 \\ +1 \end{bmatrix}, \end{aligned} \tag{24}$$

where the candidate functions - $\delta F_{i,j,k}(t)$ - are chosen from the set:

$$\boldsymbol{\delta F}^{set}_{i,j}(t) = \{\, \Delta T_{i,j}(t),\ Q(t),\ t \,\}.$$

For the plant of Fig. 2, the complete discrepancy model can be approximated using the concetanated vectros $\boldsymbol{\delta\dot{X}}$ and $\boldsymbol{\Theta(\Delta T, u, t)}$ similar to the matrix in Eq. 22.

To find the best representative vector $\boldsymbol{\xi}$, an optimization problem is formulated as:

$$\boldsymbol{\xi} = \underset{\boldsymbol{\xi}}{\operatorname{argmin}} \left(\left\| \boldsymbol{\delta\dot{X}} - \boldsymbol{\Theta(\Delta T, Q, t)}\, \boldsymbol{\xi} \right\|_2^2 \right). \tag{25}$$

This optimization problem can be analytically solved as:

$$\xi = (\boldsymbol{\Theta}^\top \boldsymbol{\Theta})^{-1} \boldsymbol{\Theta}^\top \boldsymbol{\delta\dot{X}}. \tag{26}$$

4. SIMULATION RESULTS

In this section, we compare the performance of the discrepancy model approximation of two approaches w.r.t. that of the true dynamics and the available mechanistic model in a simulated experiment.

In Table 1 the system parameter values of the true model are presented.

Table 1. Model Parameters

$\lambda_0 = 10\ J/s/K$	$\nu = 2.4e-4\ Pas$
$k_r = 0.0002$	$k_d = 10$
$R = 8.314\ J/mol/K$	$E = 10000\ J/mol$
$T_{ref} = 298\ K$	$h_{ref} = 0\ J/kg$
$V = 0.002\ m^3$	$\bar{V} = 0.005\ m^3$
$\rho = 997\ kg/m^3$	$\bar{\rho} = 997\ kg/m^3$
$c_p = 4185\ J/kg/K$	$\bar{c}_p = 4185\ J/kg/K$
$Q = [0.005 \quad 0.007]\ kg/s$	$\bar{Q} = [0.002 \quad 0.004]\ kg/s$
$h_{in} = [8370 \quad 175770]\ J/kg$	$\bar{h}_{in} = [175770 \quad 343170]\ J/kg$

Fig. 3 presents the inlet-specific enthalpies (h_{in} and $\bar{h}_{in}$) and the flowrates (Q and $\bar{Q}$) of the tube (blue) and shell (red). In the simulation studies, we assume that all the states are measured and output responses are corrupted by

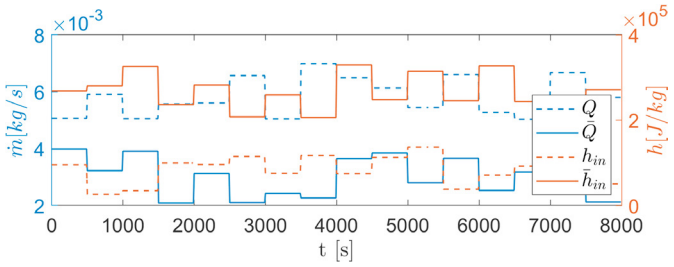

Fig. 3. Input profiles for the identification experiments

white noise with an SNR level equal to 100, where the SNR is defined as the ratio between the output signal power and the output signal noise power for our case.

The state's derivatives of the measured enthalpies are approximated via the first-order numerical derivative (Euler's method). To differentiate a signal without increasing the noise power, we smooth the raw data using the Savitzky-Golay filter.

Before the identification experiments, we generated 2 independent output measurement sets with the same noise realization, using different input signals. The first set is only used for identification methods. The second set is kept as a test set to measure the performances of the mechanistic and proposed hybrid models. Figures presented in this section show the performance of the models at the test set. The simulations experiments are conducted over the series interconnected HEN at Fig. 2.

Over the constructed data matrix $\boldsymbol{\Theta(\Delta T, T^s, Re)}$ in Sec. 3.3, we can perform identification via SINDYc extended with CPSS as described in Sec. 2.1. The corresponding identified discrepancy model via the sparse estimator for the HM I is:

$$\delta\hat{\dot{x}}^{H_1}_{i,j}(t) = 2.5 \cdot 10^{-6} \cdot Re_{i,j}(t) T^s_{i,j}(t) \Delta T_{i,j}(t) \begin{bmatrix} -1 \\ +1 \end{bmatrix}.$$

Similar to HM I, we can obtain the discrepancy model over the constructed data matrix $\boldsymbol{\Theta(\Delta T, Q, t)}$ in Sec. 3.4 via Least Square Estimation to get the model for HM II. The corresponding identified discrepancy model via the sparse estimator for the HM II is:

$$\delta\hat{\dot{x}}^{H_2}_{i,j}(t) = \left(1.92\Delta T_{i,j}(t) - 59.7 Q_{i,j}(t) + 8.34 \cdot 10^{-4} t\right) \begin{bmatrix} -1 \\ +1 \end{bmatrix}$$

The resulting hybrid models take the form of:

$$\hat{\dot{x}}^{H_1}_{i,j}(t) = \dot{x}^{M}_{i,j}(t) + \delta\hat{\dot{x}}^{H_1}_{i,j}(t), \quad \hat{\dot{x}}^{H_2}_{i,j}(t) = \dot{x}^{M}_{i,j}(t) + \delta\hat{\dot{x}}^{H_2}_{i,j}(t).$$

Fig. 4 presents the comparison of the true and the predicted enthalpy derivatives of the mechanistic model, HM I, and HM II. In the figure, due to lack of space, only the trajectories that represent the milk outlet states (i.e. 3^{rd} the compartment of the 2^{nd} heat exchanger in the cold side, $\dot{H}_{2,3}$) are displayed. Besides, the outlet state is the most relevant to the practical application in the process industry. From Fig. 4 we can realize that compensation of the mechanistic model via the identified discrepancy dynamics has improved estimation capacity w.r.t. the derivative estimation of the mechanistic model, as expected.

Since the hybrid models are in the form of ODEs, we can simulate the enthalpy trajectories of hybrid models,

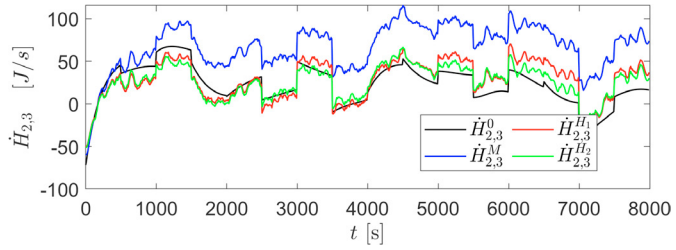

Fig. 4. Enthalpy derivative comparisons of the models at the 2^{th} HEX 3^{rd} compartement

mechanistic models, and the true systems initiated with any initial conditions and any test input signals. The simulated trajectories for the outlet state of the cold side - $H_{2,3}$ - are presented in Fig. 5. This shows that an improved forecasting performance w.r.t. the dynamic simulation of the mechanistic model can be obtained in the hybrid models that are compensated by the learned discrepancy dynamics.

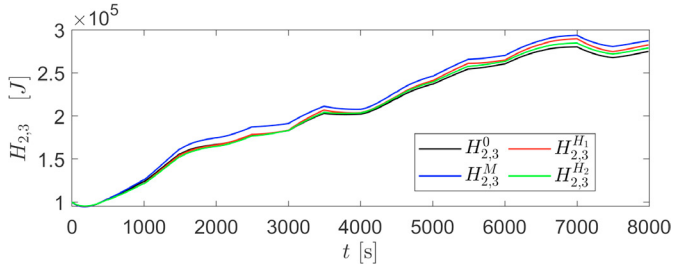

Fig. 5. Enthalpy comparisons of the models at the 2^{th} HEX 3^{rd} compartement

Fig. 6 presents the mean square error of the mechanistic and hybrid modeling approaches w.r.t. the true state values at all compartments. Simulation results of the first 4 compartments of HM I have higher accuracy w.r.t. the HM II, while HM II has higher accuracy for the last two states of the cold pipe compartments. Nevertheless, both the developed hybrid models present an improved accuracy for all compartments w.r.t. the mechanistic model

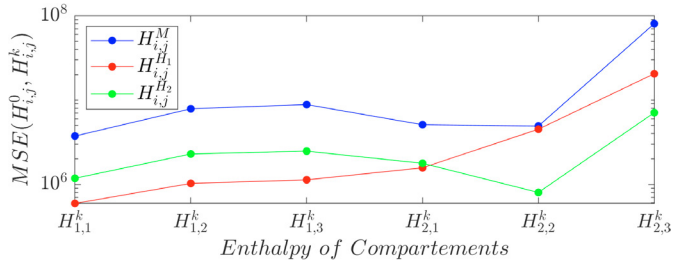

Fig. 6. Mean square error of the state predictions

5. CONCLUSION AND PERSPECTIVES

This paper introduced two hybrid modeling approaches to address the disparity between existing knowledge on heat exchanger dynamics and process measurements. The first method utilizes surface temperature and Reynolds number of the fluid in the cold tube to construct the data matrix in the hybrid discrepancy model. The second method constructs its data matrix using temperature difference between hot and cold fluids, inlet flow rate of the cold tube, and time. Both approaches enhance simulation accuracy compared to initial heat exchanger dynamics.

We acknowledge the limitations of the proposed discrepancy modeling methods. Both approaches assume that internal states can be calculted based on measurable temperatures, but in reality, only some outlet temperatures are usually measured. Describing fouling phenomenon solely with temperature and flow rates may be inadequate due to complex biochemical interactions. Additionally, numerical derivation amplifies noise effects in measured signals, which we address by smoothing with a Savitzky-Golay filter, though this may introduce bias.

The future work will focus on utilization of discovered hybrid models on control of heat exchanger network and improving the estimation of time derivatives by use of a methodology similar to DeepMod.

REFERENCES

Bansal, B. and Chen, X.D. (2006). A critical review of milk fouling in heat exchangers. *Compre. rev. in food science and safety*, 5(2), 27–33.

Both, G.J., Choudhury, S., Sens, P., and Kusters, R. (2021). Deepmod: Deep learning for model discovery in noisy data. *J. of Computational Physics*, 428, 109985.

Boxler, C. (2014). *Fouling by milk constituents and cleaning of modified surfaces*. Ph.D. thesis.

Brunton, S.L., Proctor, J.L., and Kutz, J.N. (2016). Sparse identification of nonlinear dynamics with control (sindyc). *IFAC-PapersOnLine*, 49(18), 710–715.

Ebers, M.R., Steele, K.M., and Kutz, J.N. (2022). Discrepancy modeling framework: Learning missing physics, modeling systematic residuals, and disambiguating between deterministic and random effects. *arXiv:2203.05164*.

Fryer, P. (1988). The fouling of heat exchanger networks. 511–527.

Jonsson, G.R., Lalot, S., Palsson, O.P., and Desmet, B. (2007). Use of extended kalman filtering in detecting fouling in heat exchangers. *International Journal of Heat and Mass Transfer*, 50(13-14), 2643–2655.

Kaheman, K., Kaiser, E., Strom, B., Kutz, J.N., and Brunton, S.L. (2019). Learning discrepancy models from experimental data. *arXiv preprint arXiv:1909.08574*.

Meinshausen, N. and Buhlmann, P. (2010). Stability selection. *Journal of the Royal Statistical Society: Series B (Statistical Methodology)*, 72(4), 417 473.

Rajulapati, L., Chinta, S., Shyamala, B., and Rengaswamy, R. (2022). Integration of machine learning and first principles models. *AIChE Journal*, 68(6), e17715.

Rasmussen, C.E. (2003). Gaussian processes in machine learning. In *Summer school on machine learning*, 63–71. Springer.

Shah, R.D. and Samworth, R.J. (2012). Variable selection with error control: another look at stability selection. *Journal of the Royal Statistical Society: Series B (Statistical Methodology)*, 75(1), 55 80.

Tu, J.H. (2013). *Dynamic mode decomposition: Theory and applications*. Ph.D. thesis, Princeton University.

Zitte, B., Hamroun, B., Couenne, F., and Pitault, I. (2018). Representation of heat exchanger networks using graph formalism. *IFAC-PapersOnLine*, 51(3), 44–49.